The Open-Ocean Side of the Malvinas Current in Argo Floats and 24 Years of Mercator Ocean High-Resolution (1/12) Physical Reanalysis

Camila Artana, Jean-Michel Lellouche, Nathalie Sennéchael, Christine Provost

▶ **To cite this version:**

Camila Artana, Jean-Michel Lellouche, Nathalie Sennéchael, Christine Provost. The Open-Ocean Side of the Malvinas Current in Argo Floats and 24 Years of Mercator Ocean High-Resolution (1/12) Physical Reanalysis. Journal of Geophysical Research. Oceans, 2018, 123 (11), pp.8489-8507. 10.1029/2018JC014528 . hal-02190735

HAL Id: hal-02190735
https://hal.science/hal-02190735

Submitted on 26 Sep 2019

HAL is a multi-disciplinary open access archive for the deposit and dissemination of scientific research documents, whether they are published or not. The documents may come from teaching and research institutions in France or abroad, or from public or private research centers.

L'archive ouverte pluridisciplinaire **HAL**, est destinée au dépôt et à la diffusion de documents scientifiques de niveau recherche, publiés ou non, émanant des établissements d'enseignement et de recherche français ou étrangers, des laboratoires publics ou privés.

The open-ocean side of the Malvinas Current in Argo floats and 24 years of Mercator Ocean high resolution (1/12) physical reanalysis.

Camila Artana[1], Jean-Michel Lellouche[2], Nathalie Sennéchael[1] and Christine Provost[1].

[1] : Laboratoire LOCEAN-IPSL, Sorbonne Université (UPMC, Univ. Paris 6), CNRS, IRD,MNHN, Paris, France.

[2] : MERCATOR-OCEAN, Parc Technologique du Canal, 8-10 rue Hermes, Ramonville Saint Agne, France.

Key points:

- Polar waters recurrently feed a cyclonic recirculation region north of 49°S on the open-ocean side of the Malvinas Current
- The three-dimensional structure of "blocking" and "feeding" events at 49°S is characterized for the first time.
- A 1997-2003 salinity minimum observed in the recirculation region corresponds to a period with reduced feeding events at 49°S.

Abstract

Downstream of Drake Passage, the northern branches of the Antarctic Circumpolar Current (ACC), the Polar Front (PF) and the Subantarctic Front (SAF), veer northward and the latter forms the Malvinas Current (MC). The MC flows along the continental slope up to 38°S where it loops southward as the Malvinas Return Flow (MRF). Using 24 years of Mercator Ocean physical reanalysis outputs and Argo float data, we explore the open-ocean side of the MC. We observe the occurrence of blocking events at 49°S, a region where the MC is exposed to the warm and salty anticyclonic anomalies propagating westward along the steep slope of the Malvinas Escarpment. During these events, the MC is cut off from its source, and the MC transport is considerably reduced at 49°S. The open-ocean side of the MC is regularly supplied with cold Polar Waters from the PF. The Polar Waters accumulate and recirculate between the MC and the MRF. The water characteristics of the recirculation region change over time. The recirculation region hosts significantly lighter and fresher waters during the period 1997-2003 compared with prior and later years. The 1997-2003 salinity minimum in the recirculation region corresponds to a period with reduced feeding events at 49°S.

Plain Language Summary

The Malvinas Current (MC) is an emanation of the Antarctic Circumpolar Current (ACC). It flows along the Argentinean continental slope up to 38°S where it performs a sharp cyclonic loop and turns to the south as the Malvinas Return Flow (MRF). We show that recurrently the open-ocean side of the MC is supplied with cold Polar waters north of 49°S. These waters accumulate and recirculate between the MC and the MRF. Blocking events at 49 °S cut off the MC from the ACC. 24 years of Mercator Ocean physical reanalysis outputs show recurrent blocking and feeding events and subsequent recirculation cells. Salinity in the recirculation region showed a minimum in the water column in the 1997-2003 period. The salinity minimum corresponds to a change in the occurrence of feeding and blocking events.

1. Introduction

Downstream of the Drake Passage, the northernmost branch of the ACC, the Subantarctic front (SAF) performs an equatorward loop forming the Malvinas Current (MC). The MC flows almost 2000 km following the Patagonian continental shelf up to the latitude of 38°S where it encounters the poleward flowing Brazil Current (Figure 1a). The region of confluence of these two currents, known as the Brazil-Malvinas Confluence (BMC), presents large eddy kinetic energy levels (as high as 2000 cm^2/s^2) and eddies and meanders populate this region (Figure 1b). High eddy kinetic energy levels (~1000 cm^2/s^2) are also found in Drake Passage. Due to topographic obstacles at the Drake Passage exit, the SAF and the Polar Front (PF) deflect northward (Figure 1a). The SAF and PF exit the Scotia Sea crossing the North Scotia Ridge trough east of Burdwood Bank (~2000 m) and Shag Rocks (~3200 m) Passages respectively. Subsequently, the fronts flow over the Malvinas Plateau, where the PF turns eastward and the SAF continues its path up to the BMC where it turns southward performing a sharp cyclonic loop and forming the Malvinas Return Flow (MRF) which later joins the PF around 50°S. The North Scotia Ridge acts as a barrier to the high eddy kinetic energy from the Scotia Sea, and the rather shallow Malvinas Plateau (<3000 m) further filters out the eddy kinetic energy through dissipation and mixing (Artana et al., 2016). The Malvinas Plateau has an important impact on the structure of the PF. While the PF is steered by the bottom topography and organized in a narrow jet before crossing the North Scotia Ridge (Barré et al., 2011; Provost et al., 2011) it splits and meanders over the Malvinas Plateau. At 52°S and 47.5°W, the 2500 m and 3000 m isobaths diverge favoring the PF branching (Arhan et al., 2002). Three major branches associated with high velocity cores can be recognized there (Figure 1a): the PF-N which follows the shallow bathymetry of the Malvinas Plateau and the PF-Main (PF-M) and

100 PF-South (PF-S) which proceed toward the deeper Georgia Basin. The PF-N quite often meanders
101 and sheds eddies (Artana et al., 2018a).

102 The mean position and temporal variability of the ACC fronts in Drake Passage have been
103 largely studied using satellite altimetry and hydrographic measurements. There, the ACC fronts
104 are associated with large horizontal gradients both in potential density at 400 m and in absolute
105 dynamic topography (Provost et al., 2011). The large horizontal gradients can be associated with
106 specific isopycnals in potential density at 400 m (Provost et al., 2011) and in absolute dynamic
107 topography (Sokolov and Rintoul, 2009a; Barré et al., 2011). In a recent study, Artana et al.
108 (2018b) used model outputs from the Mercator Ocean real-time system and defined criteria in
109 potential density at model depths (380m, 451m and 541 m) and dynamic topography for MC
110 system fronts (SAF, PF-N, PF-M and PF-S) and showed that the location of these fronts inferred
111 from potential density at depth below the mixed layer is in good agreement with the front location
112 inferred from mean absolute dynamic topography.

113 The potential density criteria at 541 m marks the transition between the different water
114 masses encountered at this depth in the Southwestern Atlantic Ocean (Maamaatuiahutapu et al.,
115 1994) (Figures 1c and 1d). The lighter waters (σ_Θ<27.06, purple colors in Figures 1c and 1d)
116 corresponds to South Atlantic Central Water (SACW). The SACW is carried by the Brazil Current
117 which is delimited by the Brazil Current Front (BCF). Three varieties of Antarctic Intermediate
118 Water (AAIW) are identified at 541 m: Upper (AAIW-U, 27.06< σ_Θ <27.16, red colors in Figures
119 1c and 1d), Central (AAIW-C, 27.16< σ_Θ <27.31, yellow and orange colors in Figures 1c and 1d)
120 and Lower (AAIW-L, 27.31< σ_Θ <27.35, blue colors in Figures 1c and 1d). Finally, denser waters

121 at this depth correspond to Upper Circumpolar Deep Water (UCDW, σ_Θ >27.35, black color in
122 Figures 1c and 1d) found to the south of the PF-M.

123 The 24-year-model averaged potential density at 541 m depth (Figure 1c) shows the
124 presence of a cell with density values larger than 27.25 kg/m^3 centered at 46°S and 57°W. These
125 density values in the open-ocean side of the MC could be indicative of advection and recirculation
126 of waters from the south (Figure 1c). However, this cell is disconnected from its plausible origin.
127 The disconnection takes place between 48°S and 49°S, a region of remarkable bathymetry features.
128 At 48°S the gradient of the continental slope changes from zonal to meridional and 200 km
129 offshore the bathymetry gradient is extremely strong due to the steep slope of the Malvinas
130 Escarpment, where the sea bottom drops from 2000 to 5000 m in less than 15 km. The bathymetry
131 of this region favors the occurrence of blocking events of the MC. Around once per year,
132 anticyclonic anomalies propagating westward from the deep Argentine Basin along the Malvinas
133 Escarpment cut the MC from its source (Artana et al., 2016). During these events, the downstream
134 MC does not collapse; rather it becomes the westward limb of a recirculation cell.

135 The presence of dense water in the open-ocean side of the Malvinas Current has been
136 reported and its origin has been associated with Polar Waters advected from the South (Piola and
137 Gordon, 1989). Artana et al. (2018a) show that transport maxima at 41°S are associated with eddies
138 detached from the PF propagating along the 4000 m isobath. These results suggest that water from
139 the south of the PF is advected and recirculates between the MC and the MRF.

140 Argo floats document recirculations and blocking events of the MC. The diversity of the
141 Argo float trajectories suggests that the recirculation is variable in time and space. Of particular
142 interest are Argo floats 5900704, 6901712, 6901713, 6901716, 6901714 and 6901717. Argo float

143 5900704 entered the Argentine Basin in 2010, and during 2012 it recirculated and rejoined the MC
144 three different times around 48°S following a tortuous trajectory (Figure 2d). During 2015, five
145 Argo floats (6901712, 6901713, 6901716, 6901714 and 6901717) were deployed the same day
146 (2nd May 2015) at the same position (53.07°S, 54.29°W). However, they followed different
147 trajectories. The floats 6901712 and 6901716 followed the MC along the 1000 m isobath up to the
148 latitude of 38°S. Float 6901712 followed the 2500/3000 m isobaths and never reached 38°S
149 (Figure 2a). The Argo float 6901714 also followed the 2500/3000m isobaths and left the MC at
150 42°S but then reentered in the MC suggesting the presence of a blocking event during these days
151 (Figure 2b). The Argo float 6901717 drifted up to 41°S and then recirculated in the vicinity of the
152 MC for 120 days (Figure 2c).

153 At any location, reanalysis model outputs provide continuous three-dimensional time series
154 that integrate information from *in situ* and satellite data and from the atmospheric forcing. Here
155 we took advantage of 24-year-long global Mercator Ocean reanalysis (GLORYS12) to examine
156 the open-ocean side of the Malvinas Current, the region between the MC and the MRF. In contrast
157 to the shelf-slope side of the MC, the open-ocean side of the MC has not received much attention.
158 In particular, we study how this region is fed by Polar waters and how recirculation cells and
159 blocking events affect the MC. We first focus on years 2012 and 2015 when Argo floats followed
160 peculiar trajectories and examined in detail the thermohaline MC structure and the transport of the
161 current at different latitudes. We then extend our analysis to the 24 years of the GLORYS12
162 reanalysis to study low frequency modulations in the hydrographic characteristics of the
163 recirculations and in the occurrence of blocking and feeding events.

164 This work is organized as follows. In section 2 we present the model reanalysis and the *in situ* data
165 used in this study. In section 3 we investigate recirculation, blocking events and the MC feeding

166 using model outputs of GLORYS12 reanalysis and Argo float data during 2012 and 2015. In
167 section 4 we extend our analysis to the 24 years of GLORYS12. Finally, in section 5 we summarize
168 and conclude.

169 **2. Model outputs and data**

170 **2.1 Mercator Ocean global reanalysis**

171 We used 24 years (1993-2016) of high resolution (1/12°) global Mercator Ocean reanalysis
172 (GLORYS12) from CMEMS (Copernicus Marine Environment Monitoring Service,
173 http://marine.copernicus.eu/). GLORYS12 is based on the current real-time global forecasting
174 CMEMS system (PSY4V3, Lellouche et al., 2018). The model has 50 vertical levels with 22 levels
175 in the upper 100 m leading to a vertical resolution of 1 m in the upper levels and 450 m near the
176 bottom. The physical component of the model is the NEMO (Nucleus for European Modelling of
177 the Ocean) platform (Madec et al. 2008). The model is forced at the surface by the ECMWF
178 (European Center for Medium-Range Weather Forecasts) ERA-interim atmospheric reanalysis.
179 The model assimilates observations using a reduced-order Kalman filter with a 3D multivariate
180 modal decomposition of the background error and a 7-day assimilation cycle. Along-track satellite
181 altimetric data from CLS (Pujol et al., 2016), satellite Sea Surface Temperature and Sea-Ice
182 Concentration and *in situ* temperature and salinity vertical profiles from the CORA *in situ* database
183 (Cabanes et al., 2013; Szekely et al., 2016) are jointly assimilated. Moreover, a 3D-VAR scheme
184 provides a 3D correction for the slowly-evolving large-scale biases in temperature and salinity
185 (Lellouche et al., 2018).

186 Artana et al. (2018b) evaluated the performance of the current real-time global forecasting system
187 PSY4V3 in the Southwestern Atlantic Ocean. Ten years (2007-2016) of model outputs were

compared to assimilated satellite and Argo float data and to independent *in situ* data thatwere not assimilated. The comparison showed that the PSY4V3 system correctly reproduced the general circulation and the complex hydrographic features of the Southwestern Atlantic Ocean. We found a general agreement between GLORYS12 and PSY4V3. Compared to PSY4V3, GLORYS12V1 reanalysis uses the reprocessed atmospheric forcing coming from the global atmospheric reanalysis ERA-Interim and benefits from a few changes in the system settings about observation errors. In the region of interest, comparisons with observations showed that GLORYS12 is closer to the data than PSY4V3.

2.2 Argo floats

Argo float data retrieved from http://www.usgodea.org were used in this study. The five Argo floats from 2015 (6901712, 6901713, 6901716, 6901714 and 6901717) drifted at a parking depth of 500 db while the Argo float 5900704 had a parking depth of 1000 db. These floats provide temperature and salinity profiles between 0 and 1000 db with a typical vertical resolution of 10 db every 10 days.

3. The Open Ocean side of the Malvinas Current during 2012 and 2015: Argo floats and model outputs

To study the open-ocean side of the Malvinas Current during years 2012 and 2015 we considered a section following the 3000 m isobath (colored section in Figures 1b and 1c). This section extends 1600 km from 52°S to 42°S. Hovmöller diagrams of absolute dynamic topography and potential density at 541 m for 2012 and 2015 show the time evolution of the PF-M, PF-N and SAF along the section (Figures 3a, 3b, 3e and 3f). The density values larger than 27.35 kg/m^3 and ADT values lower than -48 cm (black colors in Figures 3a, 3b, 3e and 3f) are associated with waters from the

South of the PF-M. Density values between 27.35 kg/m^3 and 27.31 kg/m^3 and ADT values between -48 and -34 cm (blue in Figures 3b and 3f green in Figures 3a and 3e) are associated with waters located between the PF-N and PF-M. Density values between 27.31 kg/m^3 and 27.16 kg/m^3 (yellow and orange colors in Figures 3b and 3f) and ADT values between -34 and 0 (yellow colors in Figures 3a and 3e) are associated with waters located between the PF-N and SAF. Density values between 27.16 kg/m^3 and 27.06 kg/m^3 and ADT between 0 and 30 cm (red colors in Figures 3a and 3e, orange colors in Figures 3b and 3f) are associated with water located between the SAF and BCF. Finally, density values lower than 27.06 kg/m^3 and ADT values larger than 30 cm (purple colors in Figures 3a and 3e, red colors in Figures 3b and 3f) are associated with waters located to the north of the BCF. In general, the density Hovmöller diagram presents similar patterns to the ones observed in the ADT Hovmöller diagram.

In December 2012 a large patch of low density values (lower than 27.16 kg/m^3, red colors in Figure 3b) and large ADT values (>0 cm, Figure 3a) extending between km 500 and 800 can be identified in both Hovmöller diagrams. Maps of ADT (Figure 3c) and potential density at 541 m (Figure3d) from model snapshots for 14 December 2012 reveal that the large patch of low potential density values detected in the Hovmöller diagram corresponds to a blocking event of the MC. This blocking event is characterized by a westward intrusion of relatively high ADT (>15 cm) and low density values (<27.05 kg/m^3) between 48°S and 49°S. The density at this position is significantly lower than the record length mean (27.05 kg/m^3 vs 27.2 kg/m^3). A cyclonic recirculation cell is observed downstream of the blocking event. This recirculation cell is associated with ADT lower than -30 cm and density values larger than 27.35 kg/m^3 at 47°S 55°W.

The Hovmöller diagrams for the year 2015 (Figure 4 e and f) show the advection of waters from the south of the PF-N from -50°S to -46°S (km 0 to 900) from January 2015 to March 2015,

suggesting that waters from the south of the PF fed the open side of the MC. Maps of model ADT (Figure 4g) and potential density at 541 m (Figure 4h) for the 24th March 2015 show the northward excursion of the PF-N. While the potential density field shows a large meander of the PF-N, the ADT field only depicts an eddy shed from the PF-N at 48°S 55°W. Large potential density values (>27.31 kg/m^3) and low ADT values (<-40 cm) are found in the Hovmöller diagrams between 46°S and 40°S (km 800-900) from March to September, suggesting that water supply from the South of the PF accumulates in the region. Denser waters (>27.35 kg/m^3, black colors in Figure 3f) observed in the center of the cyclonic recirculation are probably associated with upwelling. The signal of these dense waters is weaker in the ADT Hovmöller diagram. The differences between the ADT and the potential density signal is discussed in the sections below.

3.1 The hydrographic Structure of "blocking" and "feeding" events

The mean temperature, salinity and density distribution along the section following the 3000 m isobath (Figure 4, left panels) shows that waters located to the south of the PF are characterized with low temperatures (<2.5°C) in most of the column, relatively low salinities in the first 400 m (lower than 34 psu close to the surface) and large salinity values in the following 600 m (>34.2 psu). As a consequence, the isopycnals tilt upwards towards the southern portion of the section (between km 0 and 600). Between km 600 and 1000, isopycnals deepen and the section presents temperatures larger than 3°C in the first 500 m, salinities lower than 34.2 and densities lower than 27.25 kg/m^3 (Figure 4 left panels). By the end of the section (between km 1000 and 1500) isotherms are relatively flat and salinity presents a subsurface minimum of 34.1 psu around 200 m.

The section during the blocking event of the 14 December 2012 shows a drastic change in the thermohaline structure of the water column around kilometer 500 (Figure 4 middle panels). At km 500 isopycnals deepen and density values as low as 27.3 kg/m^3 are found at 1000m depth where the mean potential density value is 27.45 kg/m$^{3.}$ The blocking event is associated with warm temperatures (as warm as 4°C at 500 m), and large salinities in the upper 300 m (larger than 34.3 psu) of the water column. During this event, the waters from the MC sink and consequently low salinity values (<34.2 psu) are found between 500 m and 1000m. Downstream of the blocking event, between km 1000 m and 1500 m, the recirculation cell detected in the ADT and potential density maps is observed. This recirculation cell corresponds to temperatures lower than 2.5 °C below 250 m depth and salinities lower than 34.2 psu in the upper 500 m leading to a doming of the isopycnals between km 600 and 1000. While the signal of the blocking event is clear in the SLA and in the potential density anomaly at 541 m (Figure 4, upper panels) the downstream recirculation signal is much stronger in the potential density anomaly at 541 m depth than in the SLA. As explained in Artana et al. (2018b) contrasts between water masses are clearer in the potential density field at 541 m than ADT which reflects integrated changes over the full-depth water column.

The section for 24 March 2015 shows a shallowing of isopycnals between km 100 and 1000 (Figure 4 right panels) compared to the mean (Figure 4 left panels). At 250 m the minimum temperature, close to 2.5°C and the low salinity values (around than 34 psu), correspond to the Winter Water characteristics from south of the PF. While the signal of this feeding event is strong in the potential density field at 500 m, it is weak in the SLA field. The amplitude of the SLA between km 500 and 1000 is not larger than 10 cm. The warm and salty waters in the first 500 m

between km 1200 and 1500 correspond to a westward intrusion of the BCF around 43°S (Figures 3h and 3g).

The feeding and blocking events are also examined along a 400 km zonal section located at 48.7 °S in the open-ocean side of the MC where blocking events are observed (blue section in Figure 1). Due to the change of orientation of the bathymetry gradient at this latitude the MC is particularly exposed to the mesoscale activity from the Argentine Basin in this region. The mean properties along this section present temperatures larger than 3.5°C in the first 500m and a surface salinity minimum of 34.1 psu between 57 °W and 54.7 °W. Isopycnals are almost flat except in the western portion of the section where they present a slight upward inclination associated with the MC (Figure 5 left panels). The MC extends up to 54.6°W.

The blocking of 14 December 2012 shows the presence of warmer (>3°C) waters between 55.5°W and 51°W in the upper 1000 m of the water column and saltier (>34.3 psu) waters in the first 250 m compared to the mean temperatures (>2°C) and salinities (>34.2 psu) (Figure 5, panels in the center column). Due to the blocking event, the isopycnals tilt upward over a shorter distance as the longitudinal extension of the Malvinas Current is reduced. The MC extends only to 55.6°W. To the east of 55.6°W isopycnals tilt downward and the amplitude of the SLA during the blocking event is larger than 30 cm (Figure 5, middle panels).

In contrast, the zonal section for the 24 March 2015 (Figure 5, right panels) shows the presence of winter waters from the south of the PF (temperatures lower than 2°C at 500m) east of 54°W. Isopycnal slopes show that the MC extends up to -54.1°W. The SLA suggests that the MC is intensified during the excursions of the Polar Front (Figures 3g and 3h).

297 Composites of vertical temperature, salinity and density sections along the 3000 m isobath and
298 along the zonal section located at 48.7°S for the blocking and feeding events of the MC over the
299 24 years of GLORYS12 were computed (composites made of 29 blocking events and 33 feeding
300 events as explained in section 4.1.). The criterion used to identy the blocking and feedings events
301 is detailed in section 4.1. The composites depict similar changes in the water column structure as
302 the ones described previously but with a blurred signal (not shown). The signal of feeding and
303 blocking events in the water column is clearer if we consider events separately. The mean
304 properties along the 3000 m isobath (Figure 4, left panels) bear the imprints of blocking and
305 feeding events and three different regions can be defined there (white vertical lines in left panels
306 from Figure 4): the Polar Zone (between km 0 and 500), the region of blocking events between
307 km 500 and 1000 and the recirculation region between km 1000 and 1500.

308 Argo float 5900704 documented the December 2012 blocking event (Figure 6b). The Argo
309 temperature profile during the blocking event presents a warming of the upper 1000 m of the water
310 column, salty waters in the first 200m and deepening of the isopycnals. The same Argo float
311 crossed a PF-eddy on the 19 July 2012 (Figure 6a). The PF-eddy located in the 46°S-48°S
312 latitudinal band was close to the open side of the MC. Then, the Argo float recorded cold waters
313 at around 300 m (<2°C) corresponding to the winter waters from the south of the PF and a rising
314 of the isopycnals. The water column structure in both cases is similar to the one reproduced by the
315 model confirming the model skills to reproduce the thermohaline structure of blocking and feeding
316 events.

317

318

3.2. Impact on the MC transport

In this section, we investigate the impact of the blocking, feeding and the subsequent recirculation events on the MC transport. We explore the vertical distribution of the along-shelf velocity component along four sections crossing the MC and estimate the transport for 2012 and 2015 years through these sections. We analyze the MC velocity vertical structure of the December 2012 blocking event and of the recirculation that follows the March 2015 feeding event.

The map of the velocity magnitude at 541 m depth for the blocking event of the 14 December 2012 (Figure 7 a) shows a sharp eastward turn most of the MC at 49°S. The offshore flow is forced by a westward intrusion of relatively high ADT between 49°S and 48°S which blocks the northward path of the MC. However, the MC still extends up to 38 °S as it becomes the western side of a recirculation cell. Particularly large velocities of the MC (larger than 30 cm/s compared to the mean) are observed in the 48°S-49°S latitudinal band on the 18 June 2015 (Figure 7 b and c). These large values do not seem to be related to an upstream intensification of the MC since low velocity values are found between 49°S and 52°S (10 cm/s lower than the mean). Instead, the large velocity values are probably associated with the cyclonic recirculation cell of polar origin located on the open-ocean side of the MC. This cell is centered at 55°W and 46°S and has a meridional extension of 3°. The time evolution of the recirculation cells is complex (not shown). The cells break into multiple pieces that interact together merging and breaking again quite often leading to a small signal of 10 cm/s in the averaged velocity field (Figure 7 c).

Transport time series in the upper 1000 m along 4 sections located at 49.4°S, 49.3°S, 46.4°S, and 44.7°S are shown in Figure 8 and the mean and standard deviation are indicated. The 49.3°S transport time series presents the largest std values during 2012 and 2015 (8.3 Sv and 8.9 Sv

341 respectively, Figures 8b and 8f) since it is the one that is more geographically exposed to the
342 influence of the anticyclonic and cyclonic anomalies coming from the deep Argentine Basin and
343 from the Polar Zone. The mean transport from 2012 and 2015 increases from South to North with
344 a local maximum at 49.3°S (39.4Sv, Figure 8g) and 46.4°S (40.1 Sv, Figure 8c). The local maxima
345 are probably associated with recirculations. The increase of MC transport means with the latitude
346 suggests the MC waters not only are supplied from upstream but also receive an important
347 contribution from the open-ocean side.

348 The MC transport time series from mid 2012 to mid 2013 over the upper 1000 m along the section
349 located at 49.4°S shows a drastic reduction of the MC transport from mid December to beginning
350 of January in relation with the occurrence of the blocking event (Figure 8a). On the 18 December
351 2012, the MC transport reaches an absolute minimum of 4 Sv at 49.4°S. At 49.3°S, 46.4°S and
352 44.7°S the transport reduces to a minimum of 19 Sv, 23 Sv and 28 Sv on the 26 December, the 19
353 January, and 20 January, respectively. The minimum in the MC transport propagates northward
354 at a speed of 0.15 m/s. However, in downstream sections (northward of -43°S) the transport does
355 not show any signal of the blocking induced minimum (not shown).

356 The MC transport time series in 2014-2015 (Figures 8e, 8f, 8g and 8h) show large values from
357 mid May to mid June 2015 as the recirculation is established, apart from time series at 49.4°S
358 which is upstream of the recirculation. The section located at 49.3°S shows the largest transport
359 during these dates. In particular, the MC transport reaches a peak of 60 Sv for the 18 June 2015
360 (Figure 8f).

361 We then explore the distribution of the along-shelf velocity component over the four sections
362 (Figure 9). The 24-year mean of velocities (Figure 9 upper panels) show values larger than 30 cm/s

363 associated with the Malvinas Current north of 49.4°S. There is a sharp increase in velocities
364 between 49.4°S and 49.3°S. The MC is organized in two jets in the two northern sections as
365 described by Piola et al. (2011). The core of the first jet is centered at 50°W above the 700 m depth.
366 The second jet is centered at 58°W above the 2000m depth.

367 The velocities over the four sections for the dates of the extreme transport minima (14 December
368 2012, 16 December 2012, 19 January 2013 and 20 January 2013, respectively) are small compared
369 to velocity mean and the structure of the MC which is disorganized (Figure 9 second row).
370 However, the sections located further downstream (north of 42.7°S) do not show a velocity
371 reduction (not shown). On the contrary, the intensity of the MC is particularly large at 42.7°S
372 during the blocking event. A velocity core of 60 cm/s is found above the 1500 isobath there (not
373 shown).

374 In contrast, on the 18 June 2015 at the same time as a recirculation cell is established (Figure 9
375 bottom panels), velocities larger than 50 cm/s in the upper 500 m are found in the 3 northern
376 sections and larger than 30 cm/s in the southernmost section. Velocities are particularly large at
377 49.3°S with values in excess of 50 cm/s in the upper 1000 m and larger than 30 cm/s between
378 54.9°W and 60.7°W.

379 **4. The Open-ocean side of the MC in 24 years of GLORYS12 reanalysis:**

380 We now examine variations in the occurrence of blocking and feeding events over the 24 years of
381 GLORYS12.

382 The Hovmöller diagram of potential density at 541 m along the section following the 3000 m
383 isobath (colored line in Figure 1) is presented in Figure 10 a with time extending over 24 years

(from 1993 to 2016). The mean potential density varies from 27.26 to 27.44 kg/m^3 along the section (Figure 10b). Between km 600 and km 1000 the mean potential density presents a local minimum of 27.24 kg/m^3. The Hovmöller diagram (Figure 10a) shows that the local minimum is associated with the occurrence of multiple blocking events (~29) characterized by particularly low density values (lower than 27.16 kg/m^3, red colors in Figure 10a). The PF-N and PF-M positions are highly variable along the section, reaching as far north as 43°S (Figure 10 a). Waters of Polar origin are supplied to the open-ocean side of the MC as pulses or feeding events as the PF-N extends north of 48°S (km 600). Large potential density values between 27.31 kg/m^3 and 27.35 kg/m^3 are recurrent between km 1000 and 1500, revealing that water supplied from the South of the PF accumulates and recirculates there. The three different regions (the Polar Zone, the blocking region and the recirculation region) observed in Figure 4 (section 3.1) stand out in the Hovmöller diagram (their limits are indicated with black dashed line in Figure 10 a). Over the 24 years of GLORYS12 reanalysis, the feeding event from 2015 appears as a particularly important and long-lasting (~three months) episode. A low frequency modulation is observed in the occurrence of blocking and feeding events and in the water properties in the recirculation region.

4.1 Variations in the occurrence of blocking and feeding events:

To examine low frequency modulations in the occurrence of blocking and feeding events, we computed a time series of potential density at 541 m averaged over a box located between latitudes 49°S and 48°S and longitudes 56°W and 53°W (blue box in Figure 1 c) (Figure 10 c). The episodes during which the 541 m potential density anomaly is larger (respectively lower) than the standard deviation are considered as feeding (respectively blocking) events of the MC (red and blue peaks in Figure 10c). This criterion selects 29 blocking and 33 feeding events. The first years of the time series (from 1993-1996) present recurrent feeding events (densities larger than 27.25 kg/m^3) and

only two blocking events (Figure 10c). Between 1997 and 2003 the occurrence of blocking events increases to 8 while the number of feeding events is reduced to 2. In the following years, between 2004 and 2016, the number of blocking and feeding events increases considerably (19 blocking events and 23 feeding events, Figure 10c).

4.2 Variations in water characteristics in the recirculation region.

The 541 m potential density Hovmöller diagram along the section following the 3000 m isobath (colored section in Figure 1) shows a low frequency modulation in the recirculation region (between km 1000 and 1500) (Figure 10 a). The recirculation region hosts denser waters during the first 4 years of the reanalysis (1993-1996), lighter waters between 1997 and 2003 and denser waters after 2004.

Differences of the mean properties between periods 1997-2003 and 1993-1996 and between periods 2004-2016 and 1993-1996 over the 3000 m isobath section are shown in Figure 11 (the record length mean properties over the section are shown in Figure 4). The differences of the mean properties present distinct features above and below the 500 m depth. The temperature difference panels (Figure 11 a and b) show a warming pattern below 500 m and a general cooling above. The noticeable warming at 100 m in the blocking region (Figure 11b) is associated with the increase of blocking events during 2004-2016 (as shown in Figure 4, blocking events are associated to warm anomalies). The salinity difference panels (Figures 11c and 11d) show a general freshening in the upper 500 m and a change in sign below 500 m. Indeed, the 1997-2003 period corresponds to a minimum in salinity (>-0.03 psu in the recirculation region below 500 m), whereas 2004-2016 mean salinity values are larger than the first years (1993-1996). As salinity changes dominate

potential density changes, patterns in potential density and salinity differences are similar (Figure 11c, d, e and f).

In contrast to the blocking and recirculation regions, the southern portion of the Polar Zone (between km 0 and 150) does not experience much change in potential density and salinity at depths below 500 m. This suggests that the observed salinity and potential density minimum in the recirculation and blocking region below 500 m are not related to changes in the properties of the Polar Waters. Instead, they correspond to changes in the occurrence of the feeding and blocking events. The freshening in the 1997-2003 period is most likely related to a reduction in the occurrence of feeding events (Figure 10c).

Maps of model mean temperature, salinity and potential density for each period (1993-1996, 1997-2003 and 2004-2016) at 541 m confirm that waters in the recirculation region between the MC and the MRF are denser during 1993-1996, lighter during 1997-2003 and denser again after 2004 (Figure 12). They also show that changes in potential density at 541 m in the recirculation region during the 1997-2003 period are contemporaneous with a freshening of the AAIW-U flowing along the Argentinean slope. The salinity composite map from the subsequent period shows that during 2004-2016 these AAIW-U are even fresher. These AAIW-U salinity changes are consistent with the upper layer freshening observed in Figures 11c and 11d.

5. Summary and conclusions:

Argo floats and 24 years of Mercator Ocean global reanalysis outputs provide valuable information on the open-ocean side of the Malvinas Current. We first focused on years 2012 and 2015 as Argo floats documented recirculation, blocking and feeding events in these years. The GLORYS12 reanalysis provides a 4D view of the ocean state and integrates satellite and *in situ* information.

This reanalysis was used to put the Argo float data in a larger spatial and temporal context, and to document the three-dimensional structure of these events. Blocking events are associated with warm and salty anticyclonic anomalies propagating from the deep Argentine Basin and interacting with the open side of the MC. During these events, the MC is cut off from its source, the ACC at the 48°S-49°S latitude band. However, further downstream the MC does not collapse but becomes the western boundary of a cyclonic cell. During the December 2012 blocking event, the MC transport was reduced to 4 Sv at 49°S. The MC transport anomaly initially at 49°S propagates northward at a velocity speed of 0.15 m/s (in agreement with Artana et al., 2016). However, it does not reach latitudes north of 43°S and the effect of the blocking event on the MC transport is relatively local. The origin of blocking events remains uncertain. Backward trajectories of Lagrangian particles in GLORYS12 did not lead to conclusive results: tracking back the anticyclonic anomalies in the Argentine Basin is a difficult task, due to the intense mesoscale activity.

Feeding events are associated with the excursion of the PF-N to the north of 49°S, supplying cold (<2.5 °C) waters to the open-ocean side of the Malvinas Current. These waters accumulate and recirculate between the MC and the MRF, accelerating the MC transport locally. The spatial and temporal structure of the recirculation region is complex. Several recirculations cells are often observed at different latitudes at the same time. They break and interact with each other, merging and splitting apart. The 2015 feeding event appears as a particularly important and long-lasting (~three months) episode over the 24 years of GLORYS12 reanalysis. This feeding event resulted in a maximum transport of 60 Sv at 49.3°S.

The 2004-2016 mean temperature presents a warming of 0.1 °C below 500 m, compared to the 1993-1996 mean confirming the temperature trend observed by Gille (2002) at depth. Waters above 500 m experienced a freshening over the 24 years (changes in the mean larger than 0.06 psu). The freshening is consistent with the negative salinity trend reported in the waters north of the ACC in the Southern Ocean by several studies (Böning et al., 2008; Naveira Garabato et al., 2009; Purich et al., 2018). In particular, we observed a ~0.05 psu freshening of the AAIW-U flowing along the continental slope. Yao et al. (2017) reported a freshening of the AAIW in the South Atlantic Ocean during the 2005-2015 period using Argo and hydrographic data. The authors attribute the observed freshening of AAIW in the central South Atlantic to a decrease in the transport by the Agulhas Leakage.

In contrast to the consistent freshening observed above 500 m over the 24 years, salinities below 500 m show a low frequency modulation. A salinity minimum of ~0.03 psu is observed in the recirculation region during 1997-2003. The observed changes in the water properties are consistent with variations in the occurrence of blocking and feeding events. The first years of the time series (from 1993-1996) present recurrent feeding events and a few blocking events. Between 1997 and 2003 the occurrence of feeding events is reduced and the number of blocking events increases. In the following years, between 2004 and 2016, the number of blocking and feeding events increases. The salinity minimum from 1997-2003 in the recirculation region corresponds to a reduction in the occurrence of feeding events.

Acknowledgements:

The authors are grateful to the CNES (Centre National d'Etudes Spatiales) for constant support. Camila Artana acknowledges Scholarship from Sorbonne Université (ED129). The satellite data and model outputs are available at Copernicus Marine Environment Monitoring Service (CMEMS; http://marine.copernicus.eu/). The float data were collected and made freely available by the international ARGO program and the national programs that contribute to it (http://www.argo.ucsd.edu). The ARGO program is part of the Global Ocean Observing System.

References:

Arhan, M., Naveira Garabato, A. C., Heywood, K. J., & Stevens, D. P. (2002). The Antarctic Circumpolar Current between the Falkland Islands and South Georgia. *Journal of Physical Oceanography*, *32*(6), 1914-1931.

Artana, C., Ferrari, R., Koenig, Z., Saraceno, M., Piola, A. R., & Provost, C. (2016). Malvinas Current variability from Argo floats and satellite altimetry. *Journal of Geophysical Research: Oceans*, *121*(7), 4854-4872.

Artana, C., Ferrari, R., Koenig, Z., Sennéchael, N., Saraceno, M., Piola, A. R., & Provost, C. (2018a). Malvinas Current Volume Transport at 41°S: A 24 Yearlong Time Series Consistent With Mooring Data From 3 Decades and Satellite Altimetry. *Journal of Geophysical Research: Oceans*, *123*(1), 378-398.

Artana, C., Lellouche, J. M., Park, Y. H., Garric, G., Koenig, Z., Sennéchael, N., ... & Provost, C. (2018b). Fronts of the Malvinas Current System: Surface and Subsurface Expressions Revealed by Satellite Altimetry, Argo Floats, and Mercator Operational Model Outputs. *Journal of Geophysical Research: Oceans*.

Barré, N., Provost, C., Renault, A., & Sennéchael, N. (2011). Fronts, meanders and eddies in Drake Passage during the ANT-XXIII/3 cruise in January–February 2006: A satellite perspective. *Deep Sea Research Part II: Topical Studies in Oceanography*, *58*(25), 2533-2554.

Böning, C. W., Dispert, A., Visbeck, M., Rintoul, S. R., & Schwarzkopf, F. U. (2008). The response of the Antarctic Circumpolar Current to recent climate change. *Nature Geoscience*, *1*(12), 864.

Cabanes, C., Grouazelm A., vos Schuckmann, K., Hamon, M., Turpin, V., Coatanoan, C., Paris, F., Guinehut, S., Boone, C., Ferry, N., de Boyer Montegut, C., Carval, T., Reverdin G., Pouliquen, S., Le Traon, P.Y., (2013), The CORA dataset: validation and diagnostics of in-situ ocean temperature and salinity measurements. *Ocean Sci.* 9, 1-18. Doi:10.5194/os-9-1-2013.

537 Donlon, C.J., Martin, M., Stark, J., Roberts-Jones, J., Fiedler, E., Wimmer, W., (2012). The
538 Operational Sea Surface Temperature and Sea Icea Analysis (OSTIA) system. *Remote Sensing of*
539 *Environment* 116, 140-158. doi: 10.1016/j.res.2010.10.017.
540 Gille, S. T. (2002). Warming of the Southern Ocean since the 1950s. Science, 295(5558), 1275-
541 1277.
542 Lellouche, J.-M., Greiner, E., Le Galloudec, O., Garric, G., Regnier, C., Drevillon, M., Benkiran,
543 M., Testut, C.-E., Bourdalle-Badie, R., Gasparin, F., Hernandez, O., Levier, B., Drillet, Y., Remy,
544 E., & Le Traon, P.-Y. (2018). Recent updates on the Copernicus Marine Service global ocean
545 monitoring and forecasting real-time 1/12° high resolution system, Ocean Sci.
546 https://doi.org/10.5194/os-2018-15.
547 Maamaatuaiahutapu, K., Garçon, V. C., Provost, C., Boulahdid, M., & Bianchi, A. A. (1994).
548 Spring and winter water mass composition in the Brazil-Malvinas Confluence. *Journal of Marine*
549 *Research*, *52*(3), 397-426.
550 Madec, G. (2008), NEMO ocean engine. Note du Pôle de modélisation, Institut Pierre-Simon
551 Laplace (IPSL), France, No. 27 ISSN, 1288-1619.
552 Peterson, R. G., & Whitworth, T. (1989). The Subantarctic and Polar Fronts in relation to deep
553 water masses through the southwestern Atlantic. *Journal of Geophysical Research:*
554 *Oceans*, *94*(C8), 10817-10838.
555 Piola, A. R., & Gordon, A. L. (1989). Intermediate waters in the southwest South Atlantic. *Deep*
556 *Sea Research Part A. Oceanographic Research Papers*, *36*(1), 1-16.
557 Provost, C., Renault, A., Barré, N., Sennéchael, N., Garçon, V., Sudre, J., & Huhn, O. (2011). Two
558 repeat crossings of Drake Passage in austral summer 2006: Short-term variations and evidence for

considerable ventilation of intermediate and deep waters. *Deep Sea Research Part II: Topical Studies in Oceanography*, *58*(25-26), 2555-2571.

Pujol, M.-I., Y. Faugère, G. Taburet, S. Dupuy, C. Pelloquin, M. Ablain, and N. Picot, (2016), DUACS DT2014: the new multi-mission altimeter data set reprocessed over 20 years, *Ocean Sci.*, 12, 1067-1090, doi:10.5194/os-12-1067-2016.

Purich, A., England, M. H., Cai, W., Sullivan, A., & Durack, P. J. (2018). Impacts of broad-scale surface freshening of the Southern Ocean in a coupled climate model. *Journal of Climate*, *31*(7), 2613-2632.

Naveira Garabato, A. C., Jullion, L., Stevens, D. P., Heywood, K. J., & King, B. A. (2009). Variability of Subantarctic Mode Water and Antarctic Intermediate Water in the Drake Passage during the Late-Twentieth and Early-Twenty-First Centuries. *Journal of Climate*, *22*(13), 3661-3688. DOI: 10.1175/2009JCLI2621.1

Szekely, T., Gourrion, J., Pouliquen, S., Reverdin, G., (2016). CORA, Coriolis, Ocean Dataset for Reanalysis. SEANOE doi:/http://doi.org/10.17882/46219.

Smith, W. H. F., and D. T. Sandwell (1994), Bathymetric prediction from dense satellite altimetry and sparse shipboard bathymetry, *J. Geophys. Res.,* **99,** 21 803–21 824.

Sokolov, S., & Rintoul, S. R. (2009). Circumpolar structure and distribution of the Antarctic Circumpolar Current fronts: 1. Mean circumpolar paths. *Journal of Geophysical Research: Oceans*, *114*(C11).

Yao, W., Shi, J., and Zhao, X. (2017). Freshening of Antarctic Intermediate Water in the South Atlantic Ocean in 2005–2014, Ocean Sci., 13, 521-530, https://doi.org/10.5194/os-13-521-2017.

Figure captions:

Figure 1:

Southwest Atlantic: (a) Model mean surface velocity magnitude (in cm/s) and mean surface velocities (larger than 10cm/s); (b) Mean eddy kinetic energy per unit mass (in cm^2/s^2) from GLORYS12 outputs; (c) 24-year mean model potential density at 541 m depth classified following front-detection criteria defined in Artana et al. (2018); (d) Potential temperature-salinity diagram from mean model temperatures and salinities at 541 m classified in terms of potential density criteria at 541 m. Corresponding water masses are indicated. Also indicated: the section along 3000 m isobath with color indicating the distance (in km) from its origin, a zonal blue section at 48.7°S and a blue box over which spatially averaged time series are computed (shown in Figure 10). The latitudinal limits of the box are indicated with white sections in Figure 1b. They delimit 3 geographical regions of interest: the Polar Zone, the blocking region and the recirculation region.

Bottom topography isobaths correspond to 6000, 5000, 3000, 1000 and 300 m (from Smith and Sandwell, 1994). The mean location of the Malvinas Current System as defined in Artana et al. (2018b) are indicated in black.

Figure 2:

Trajectories of 6 ARGO floats: a) Floats 6901712 (dark blue), 6901713 (green) and 6901716 (red); b) float 6901714 (light blue); c) float 6901717 (purple); d) float 5900704 (yellow), the 2012 trajectory is indicated in brown. The section along the 3000 m isobath is indicated in black.

Figure 3:

Hovmöller diagram of model ADT (a and e) and model potential density (b and f) above the 3000 m isobath showed in Figure 1. Y-axis is labelled with cumulative distance from the origin at 52°S and 48°W (in km) X-axis is time (daily resolution) with time ticks every 2 months. The dashed lines indicate the latitudinal limits of the blue box from Figure 1 c.

Model ADT (c and g) and potential density at 541 m (d and h) on the 14 th of December 2012 and 24 th of March 2015 (date marked in the Hovmöller diagrams with a vertical black line).

Figure 4:

Vertical distribution of potential temperature, salinity and potential density over the 3000 m isobath section from Figure 1 b and c (colored line). Left panels: mean over 24 years. Middle panels: section on the 14 December 2012 (blocking event). Right panels: section on 24 of March 2015 (feeding event). The black line indicates the 541 m level. Top panel: sea level anomaly (SLA in blue) and potential density anomaly (green) extracted over the section. Lower panel: bottom topography over the section. The white vertical lines in left panels delimits 3 geographical regions of interest: the Polar Zone (defined between 0and 600 km), the blocking region (between 600 and 1000 km) and the recirculation region (between 1000 and 1600 km).

Figure 5:

Vertical distribution of potential temperature, salinity and potential density over the 48.7°S section from Figure 1. Left panels: mean over 24 years. Middle panels: section on the 14 December 2012 (blocking event). Right panels: section on 24 of March 2015 (feeding event). The black line

indicates the 541 m level. The vertical white lines indicate the extension of the MC. Top panel: SLA and potential density anomaly extracted over the section. Lower panel: bottom topography.

Figure 6:

Trajectory and vertical distribution of potential temperature, salinity and potential density from float 5900704. The Trajectory of the float is superimposed on an ADT map from July 19, 2012 (a) and from December 14, 2012 (b). The location of the float at that date is shown as a white disk. Potential temperature, salinity and potential density along the trajectory are shown in c), d) and e) respectively. The profiles at the dates of a) and b) are framed in white. In b) the float is in a blocking feature, in a) within a recirculation cell.

Figure 7:

Model velocity magnitude at 541m (in cm/s) larger than 20 cm/s for (a) the 14 December 2012 and (b) the 18 June 2015 and (c) the record length mean. The corresponding front position of the PF-N, PF-M and SAF deduced from model altimetry is represented. Four sections located at 49.4°S, 49.3°S, 46.4°S and 44.7 °S crossing the MC are indicated with magenta lines.

Figure 8:

MC volume transport in the upper 1000 m computed over the four sections (magenta lines in Figure 7): 49.4°S (a and e), 49.3°S (b and f), 46.4°S (c and g) and 44.7°S (d and h). The MC transport is computed from June 2012 to June 2013 (left panels) and from September 2014 to September 2015 (right panels).

Figure 9:

Vertical distribution of along-shelf velocity components along four sections crossing the MC at 49.4°S, 49.3°S, 46.4°S and 44.7°S (magenta lines in Figure 7). Top panels show the mean over the 24 years at each section. Middle Panels show the along-shelf velocity component for the dates of extreme transport minimum at each section. The bottom panels show each section on the 18 June 2015.

Figure 10:

a) Hovmöller diagram of potential density at 541m along the 3000 m isobath section over the 24 years. Y-axis is labelled with cumulative distance from the origin at 48°W, 52°S (in km) and latitude, X-axis is time (daily resolution). b) model mean potential density along the section and standard deviation. c) Time series of potential density at 541 m averaged on the blue box from Figure 1. Values lower than the standard deviation are shaded. Black dashed lines in the Hovmöller indicate the latitudinal limits of the box and separate the Polar Zone (0-600 km), the blocking region (600-1000 km) and the recirculation region (1000-1600 km).

Figure 11:

Differences of the mean properties between the periods 1997-2003 and 1993-1996 (left panels) and between the periods 2004-2016 and 1993-1996 (right panels) over the 3000 m isobath section (colored section in Figure 1). The black lines separate the Polar Zone (0-600 km) the blocking region (600-1000 km) and the recirculation region (1000-1600). Lower panels: Bottom topography.

Figure 12:

Maps of Potential density in kg/m^3 (left panels), potential temperature in °C (center panels) and salinity in psu (right panels) at 541 m averaged over the period 1993-1996 (a, b and c), over the period 1997-2003 (d, e and f) and over the period 2004-2016 (g, h and i).

681 **Figures**

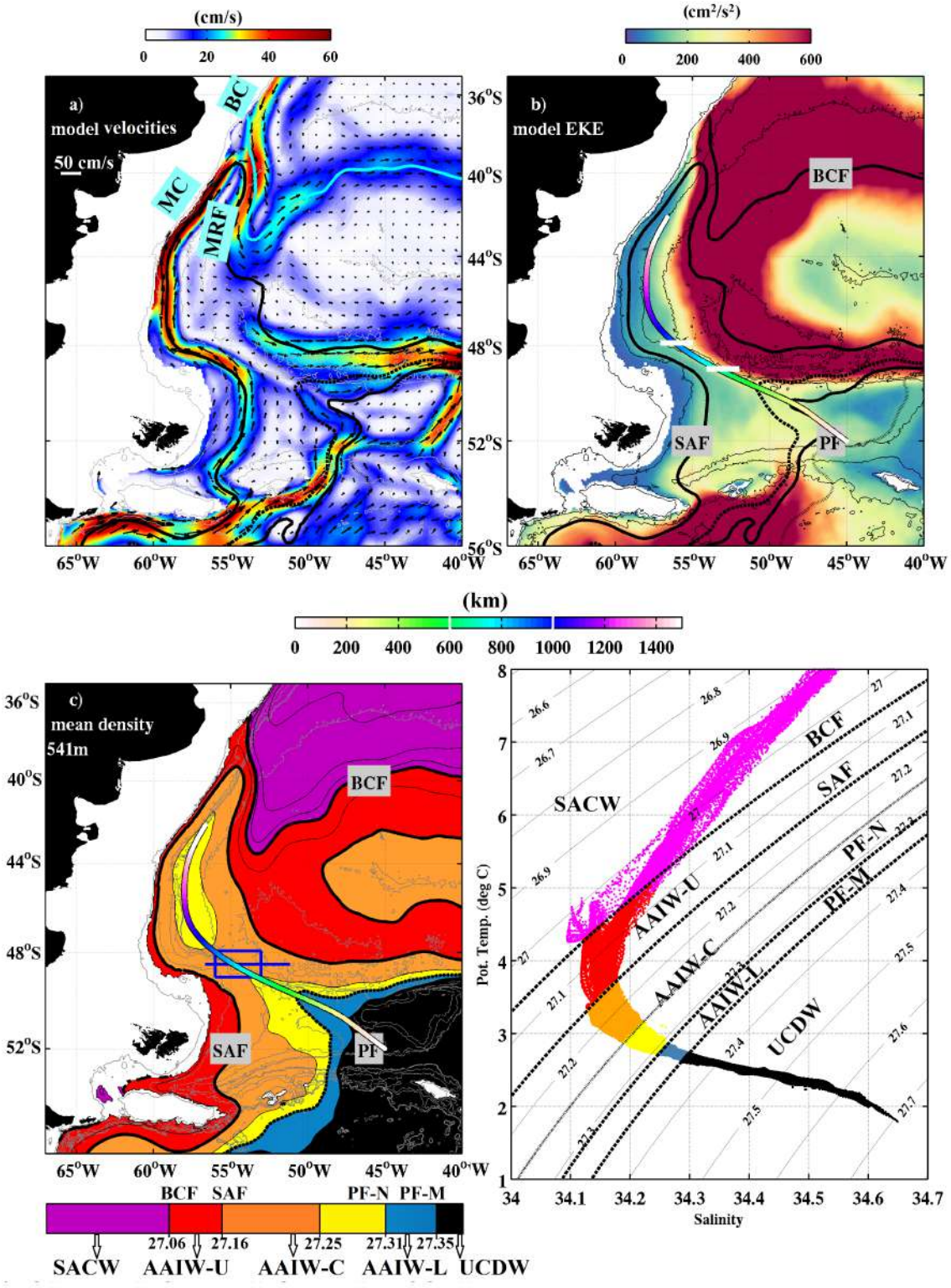

682

683 Figure 1

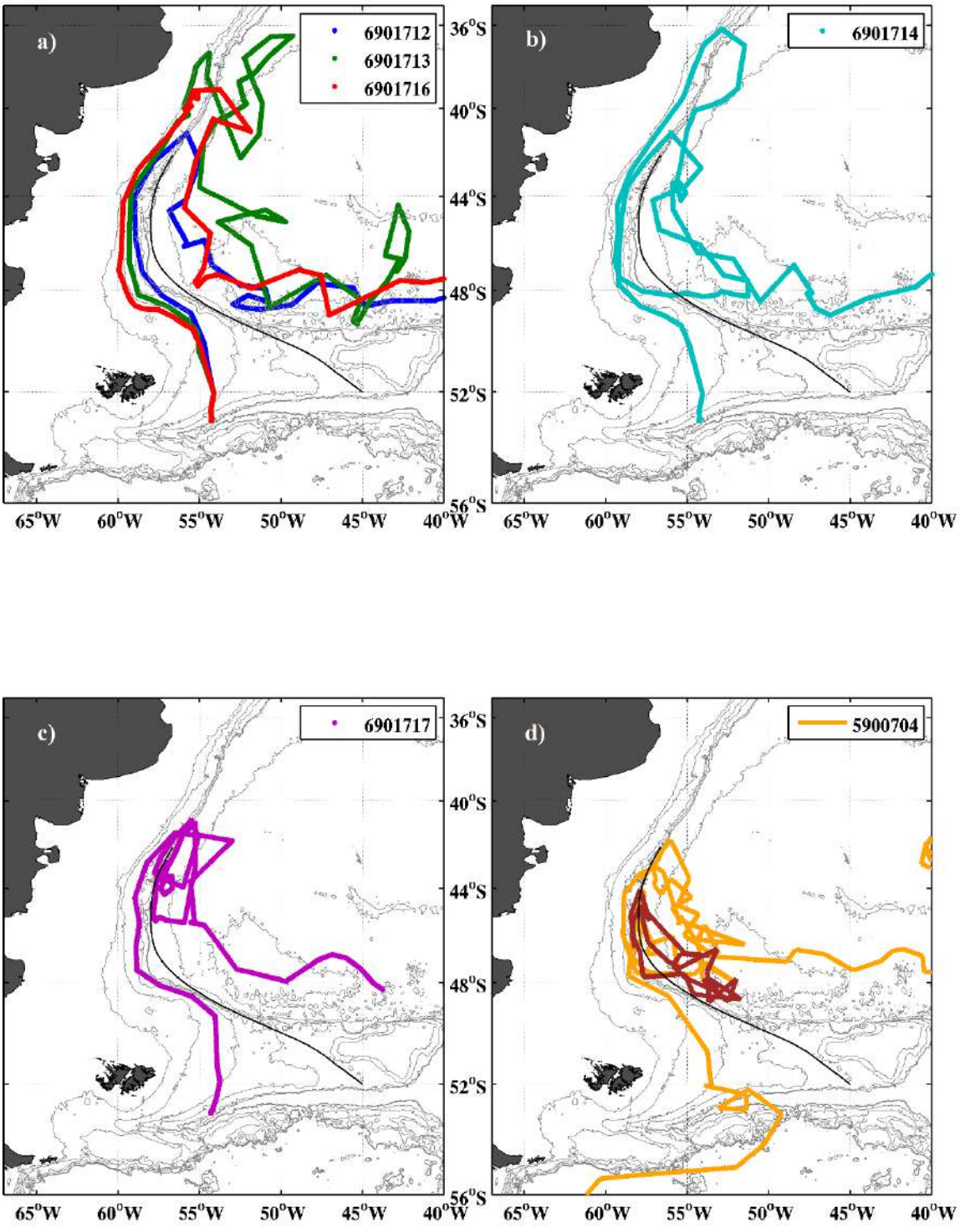

684

685 Figure 2

686

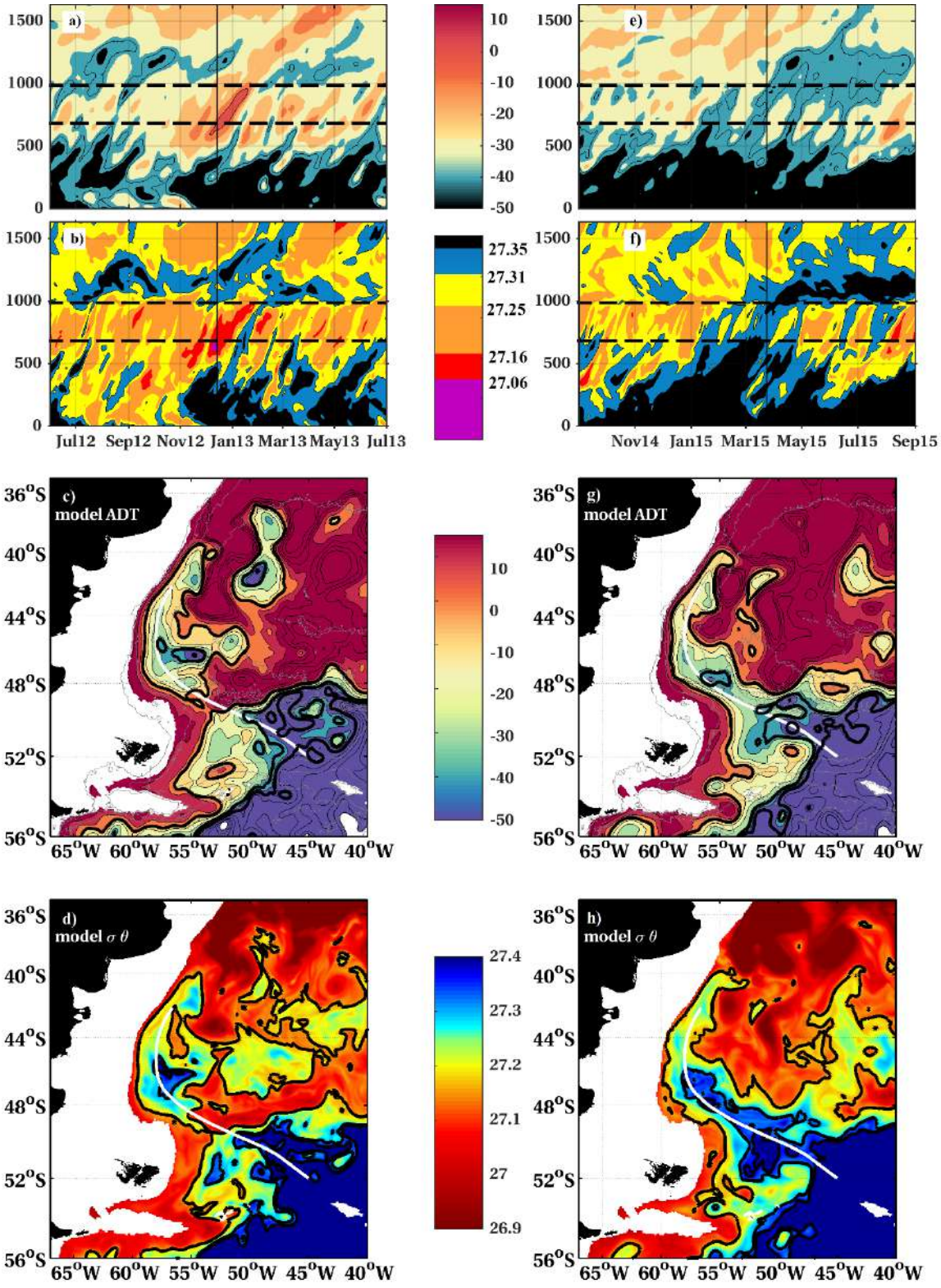

687

688 Figure 3

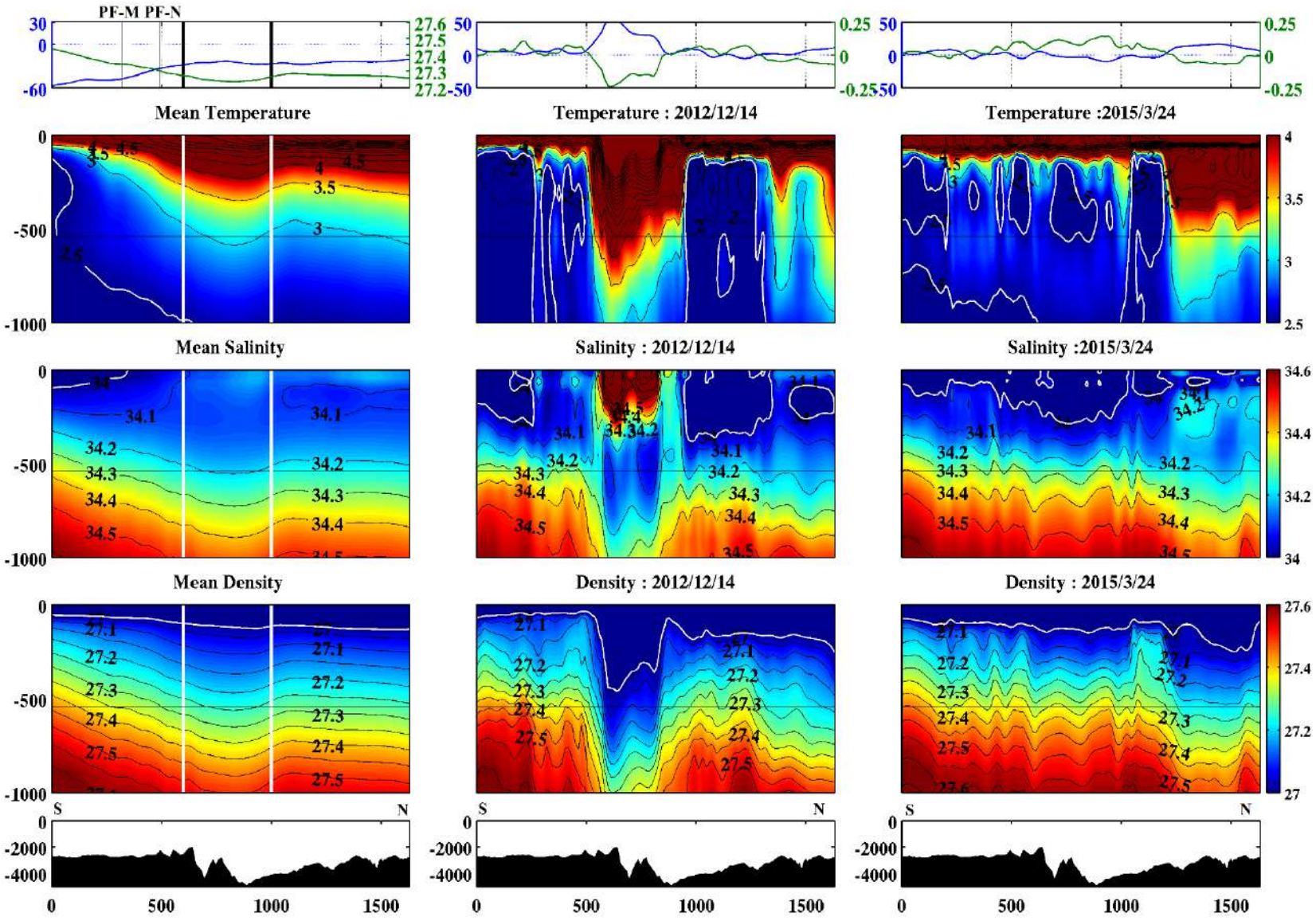
PF-M PF-N
Mean Temperature
Temperature : 2012/12/14
Temperature :2015/3/24
Mean Salinity
Salinity : 2012/12/14
Salinity :2015/3/24
Mean Density
Density : 2012/12/14
Density : 2015/3/24
S
N

Figure 4

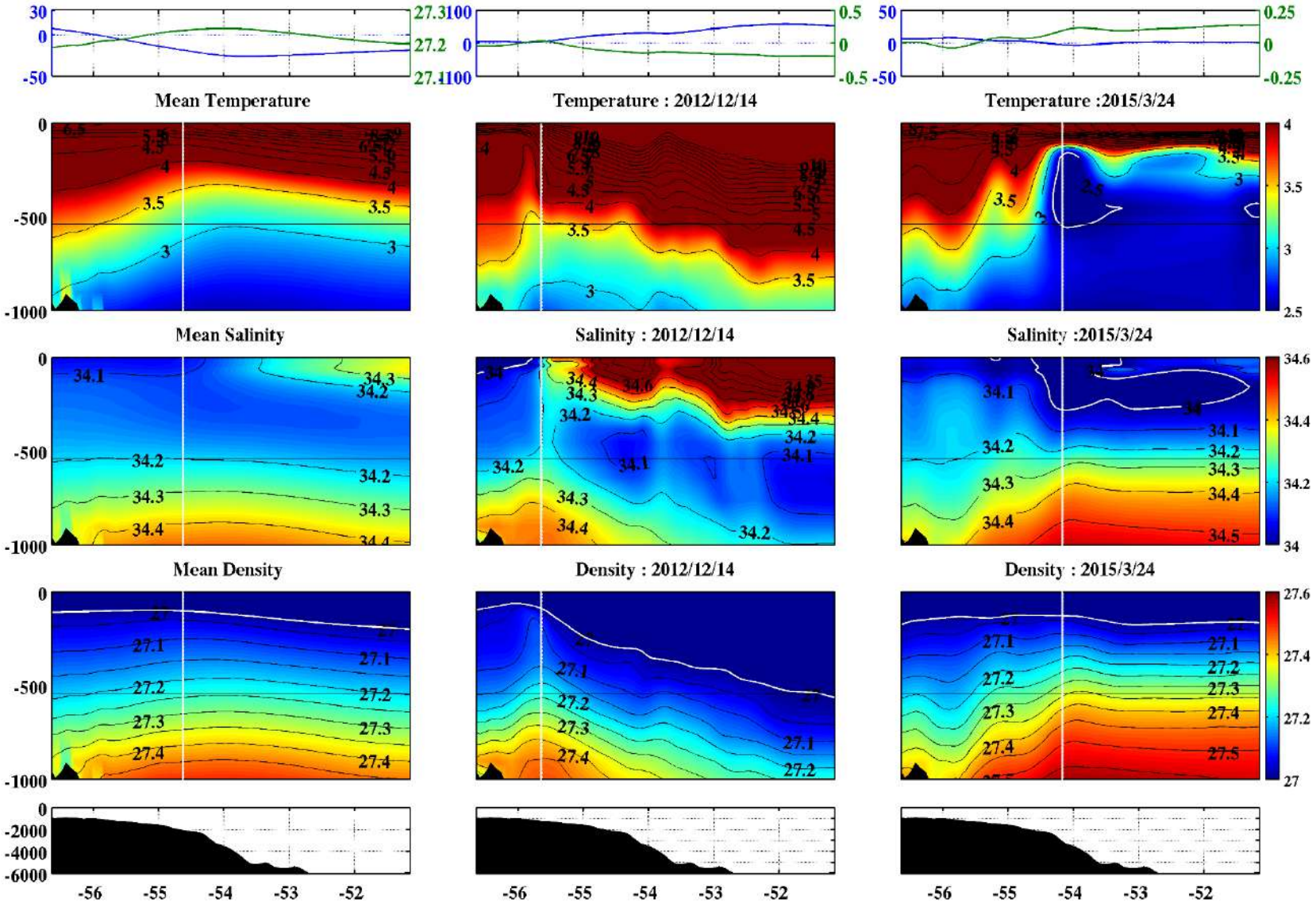
Mean Temperature
Temperature : 2012/12/14
Temperature :2015/3/24
Mean Salinity
Salinity : 2012/12/14
Salinity :2015/3/24
Mean Density
Density : 2012/12/14
Density : 2015/3/24

Figure 5

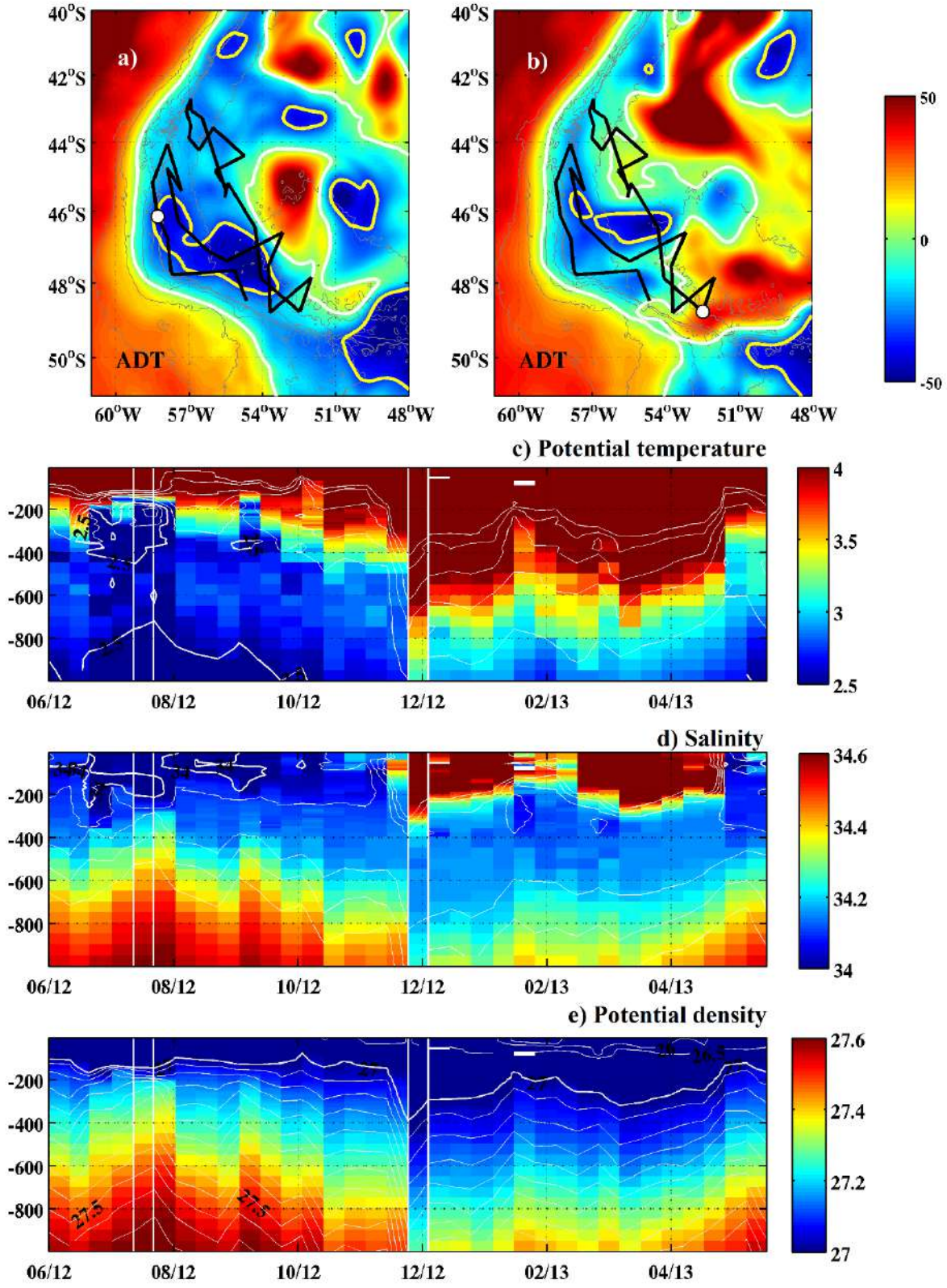
a)
b)
ADT
ADT
40°S
42°S
44°S
46°S
48°S
50°S
60°W
57°W
54°W
51°W
48°W
50
0
-50
c) Potential temperature
4
3.5
3
2.5
d) Salinity
34.6
34.4
34.2
34
e) Potential density
27.6
27.4
27.2
27
-200
-400
-600
-800
06/12
08/12
10/12
12/12
02/13
04/13

Figure 6

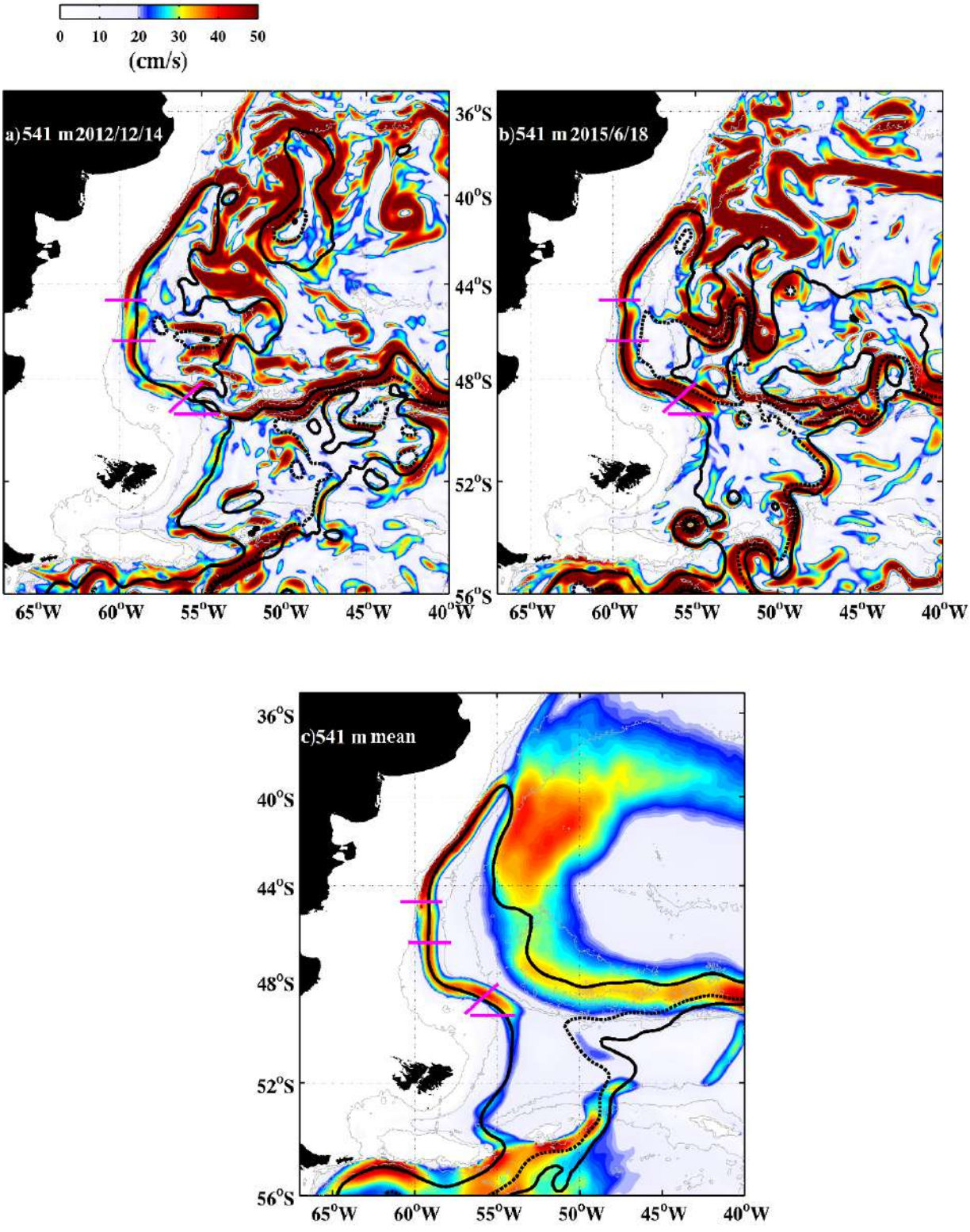
0 10 20 30 40 50
(cm/s)
a)541 m2012/12/14
b)541 m 2015/6/18
c)541 m mean
36°S
40°S
44°S
48°S
52°S
56°S
65°W
60°W
55°W
50°W
45°W
40°W

Figure 7

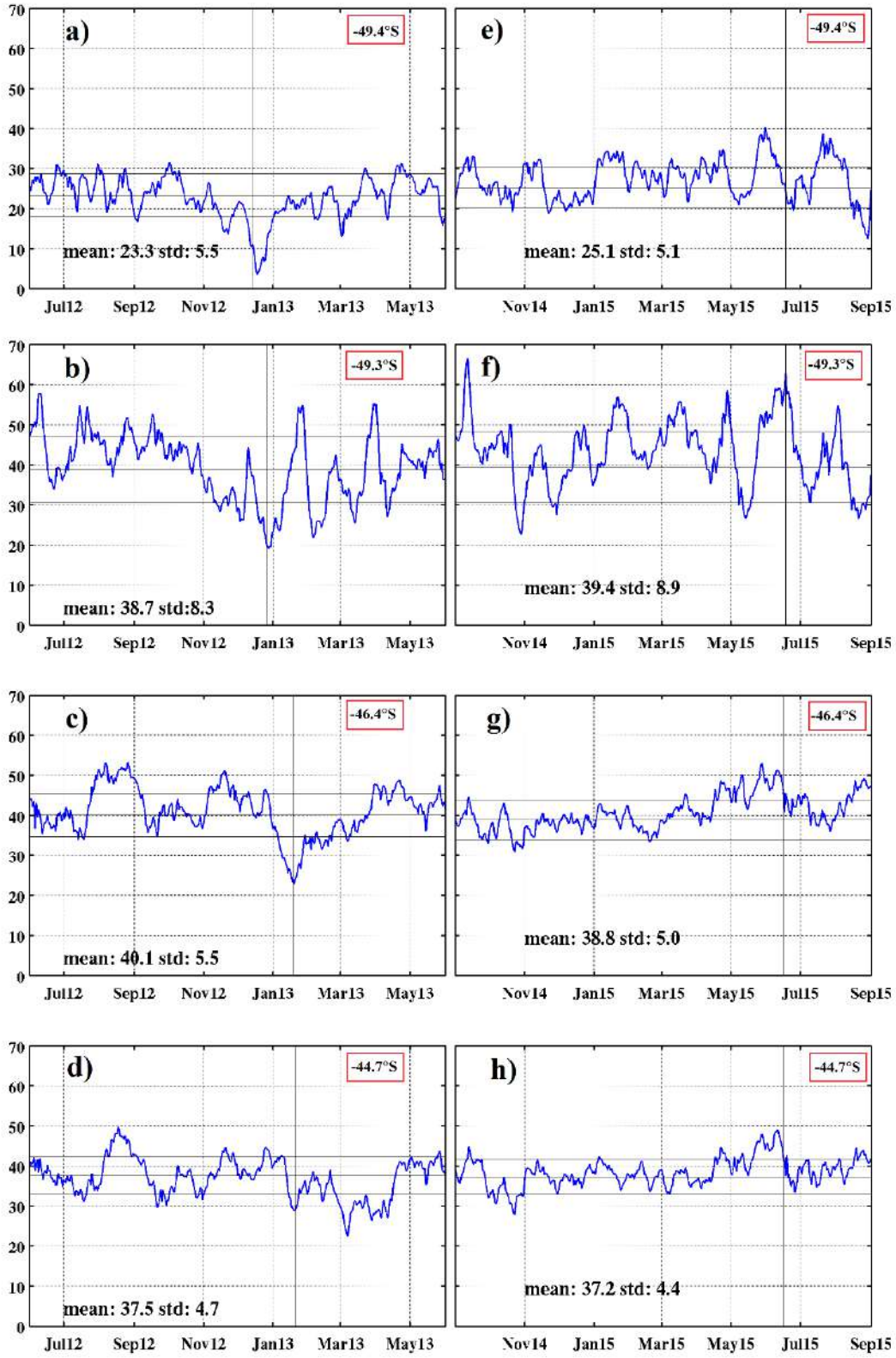
a)
-49.4°S
mean: 23.3 std: 5.5
e)
-49.4°S
mean: 25.1 std: 5.1
b)
-49.3°S
mean: 38.7 std:8.3
f)
-49.3°S
mean: 39.4 std: 8.9
c)
-46.4°S
mean: 40.1 std: 5.5
g)
-46.4°S
mean: 38.8 std: 5.0
d)
-44.7°S
mean: 37.5 std: 4.7
h)
-44.7°S
mean: 37.2 std: 4.4
0
10
20
30
40
50
60
70
Jul12
Sep12
Nov12
Jan13
Mar13
May13
Nov14
Jan15
Mar15
May15
Jul15
Sep15

Figure 8

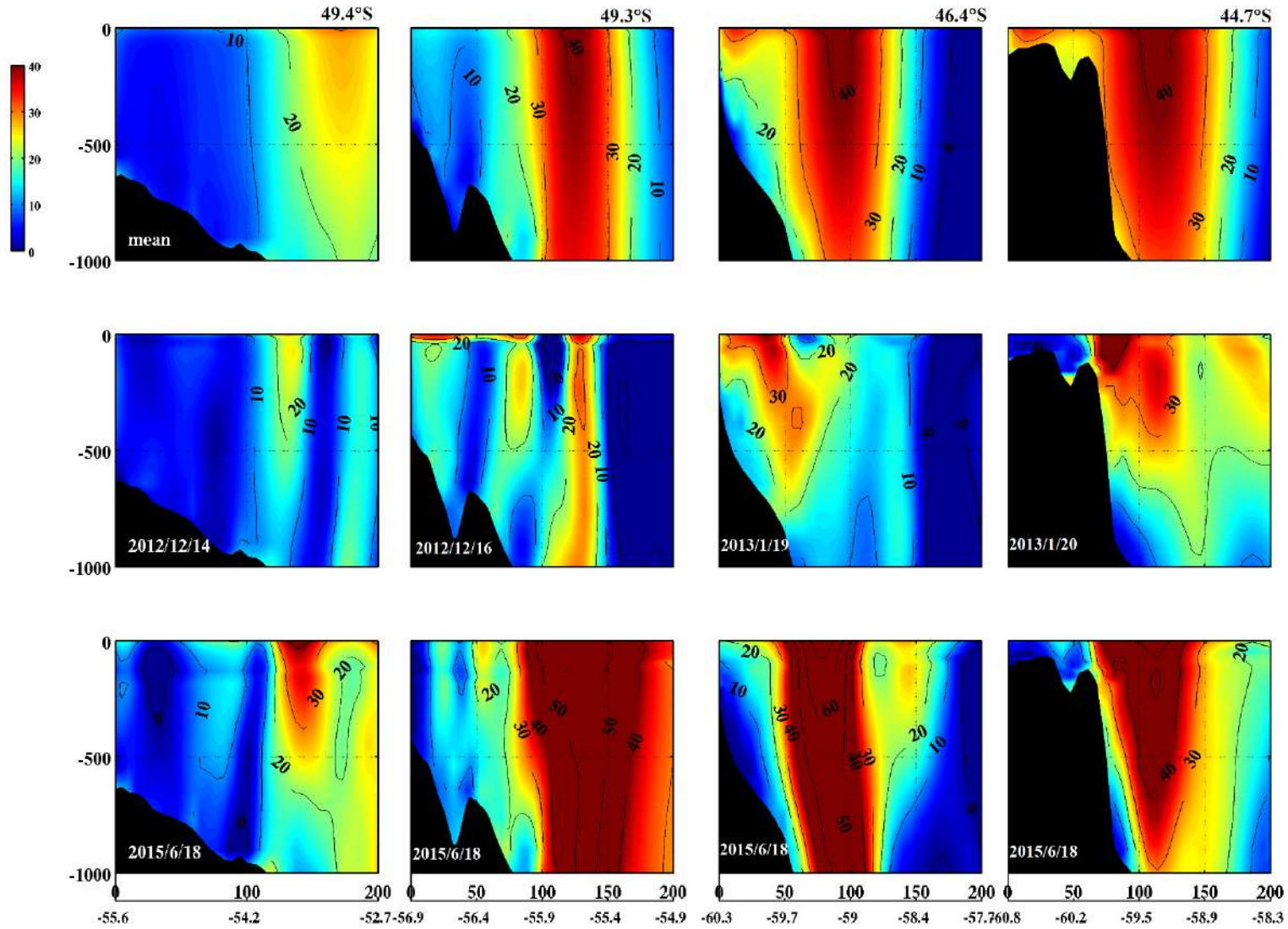
49.4°S
49.3°S
46.4°S
44.7°S
mean
2012/12/14
2012/12/16
2013/1/19
2013/1/20
2015/6/18
2015/6/18
2015/6/18
2015/6/18
0
-500
-1000
0
100
200
0
50
100
150
200
0
50
100
150
200
0
50
100
150
200
-55.6
-54.2
-52.7
-56.9
-56.4
-55.9
-55.4
-54.9
-60.3
-59.7
-59
-58.4
-57.7
60.8
-60.2
-59.5
-58.9
-58.3

Figure 9

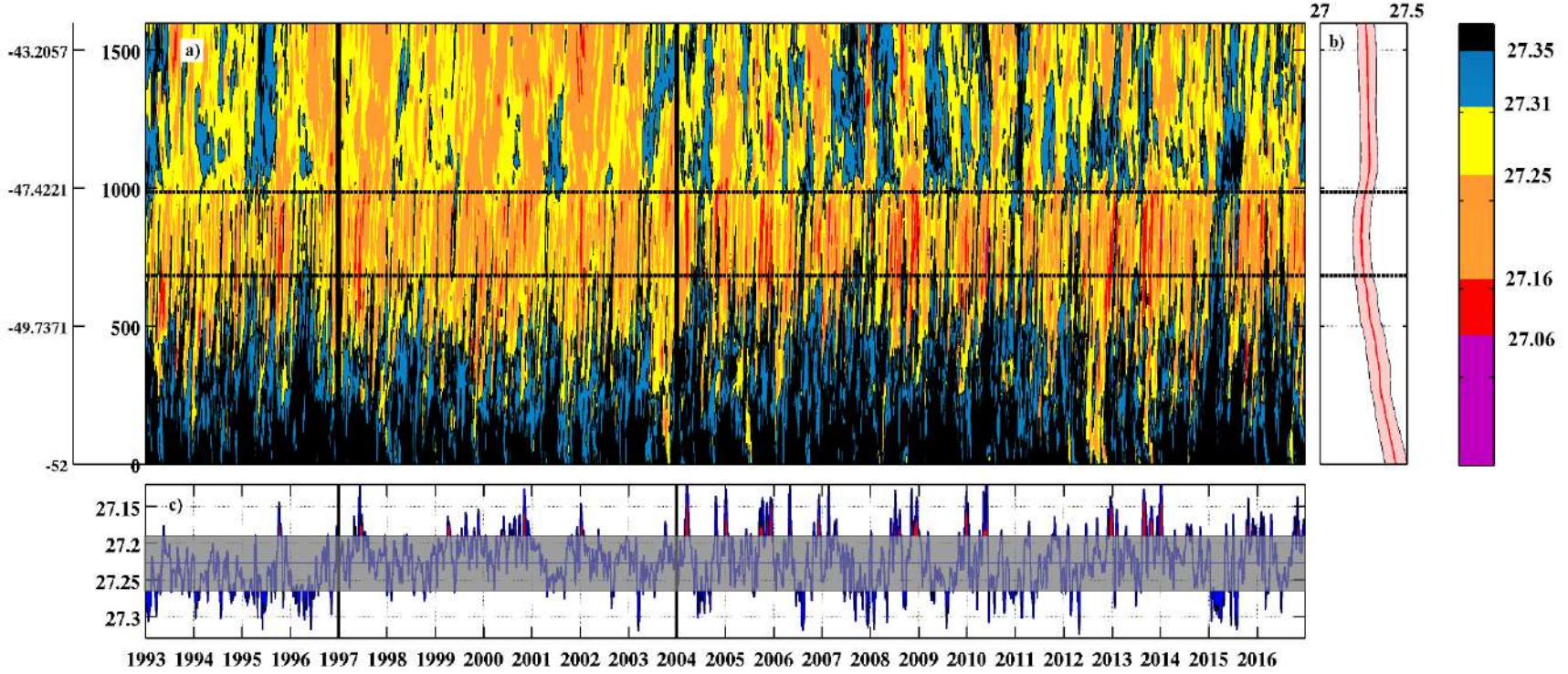
-43.2057
-47.4221
-49.7371
-52
1500
1000
500
0
a)
27
27.5
b)
27.35
27.31
27.25
27.16
27.06
27.15
27.2
27.25
27.3
c)
1993 1994 1995 1996 1997 1998 1999 2000 2001 2002 2003 2004 2005 2006 2007 2008 2009 2010 2011 2012 2013 2014 2015 2016

Figure 10

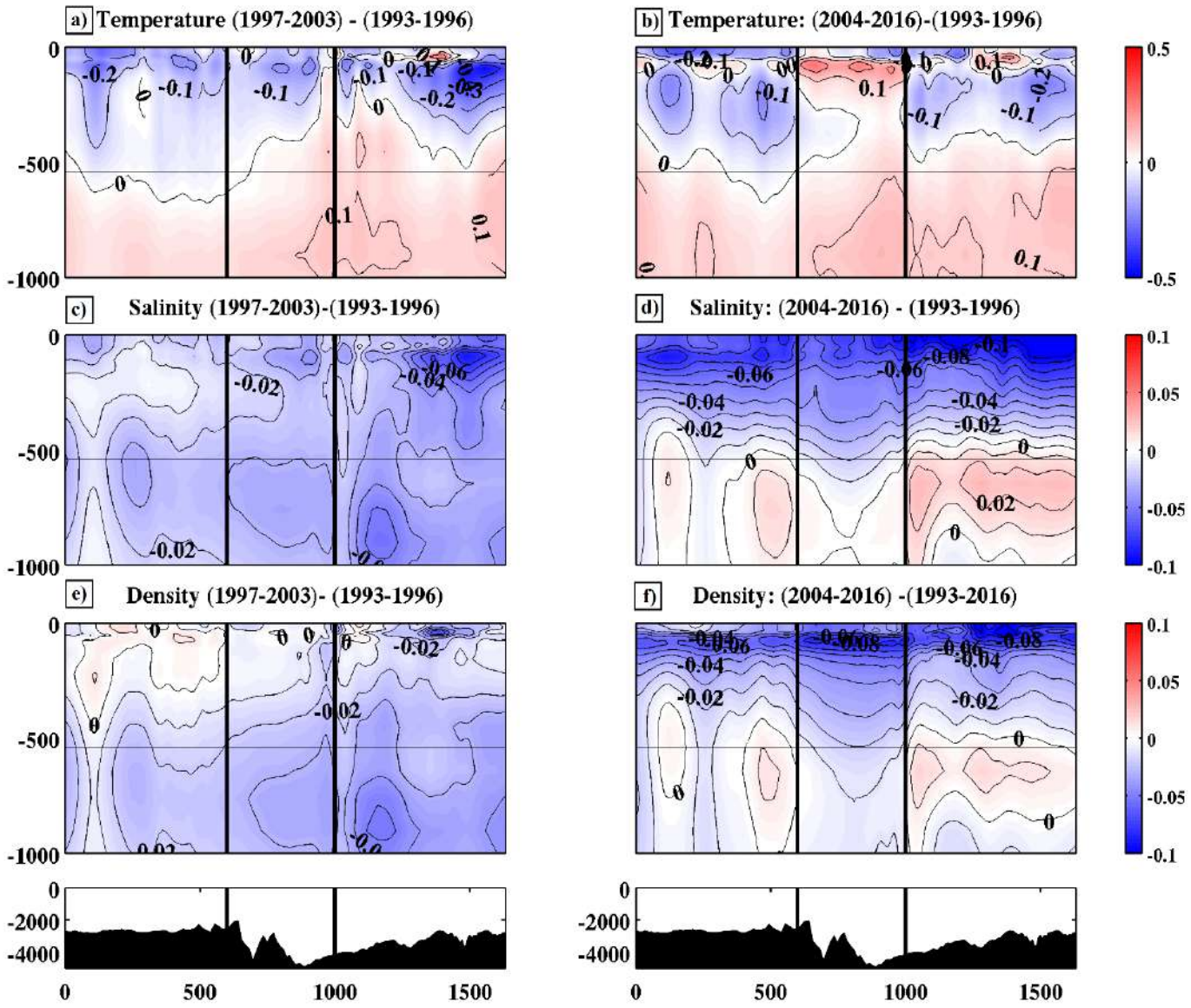
a) Temperature (1997-2003) - (1993-1996)
b) Temperature: (2004-2016)-(1993-1996)
c) Salinity (1997-2003)-(1993-1996)
d) Salinity: (2004-2016) - (1993-1996)
e) Density (1997-2003)- (1993-1996)
f) Density: (2004-2016) -(1993-2016)
0
-500
-1000
-2000
-4000
0
500
1000
1500
0.5
0
-0.5
0.1
0.05
-0.05
-0.1

Figure 11

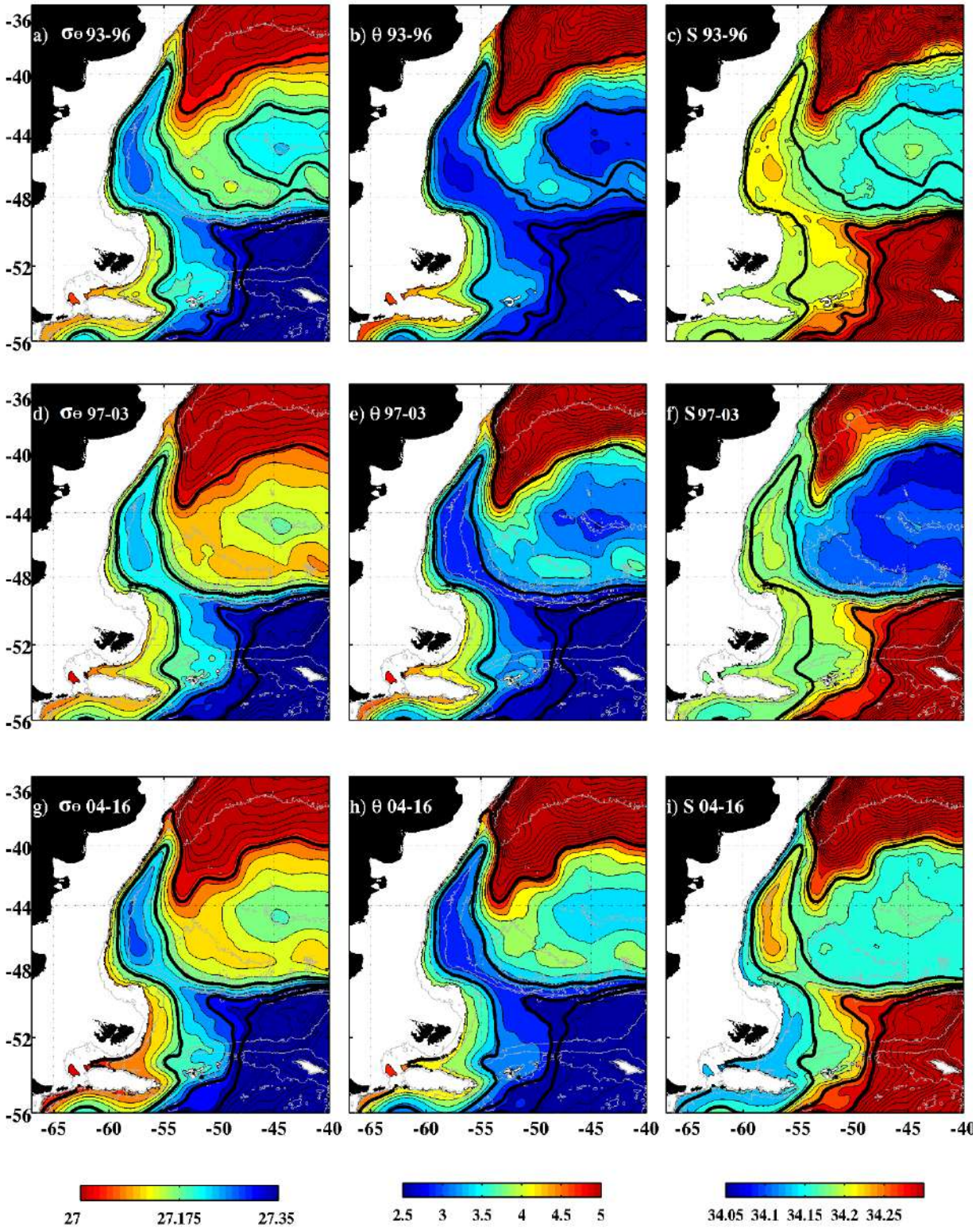
a) σθ 93-96
b) θ 93-96
c) S 93-96
d) σθ 97-03
e) θ 97-03
f) S 97-03
g) σθ 04-16
h) θ 04-16
i) S 04-16
-36
-40
-44
-48
-52
-56
-65 -60 -55 -50 -45 -40
27 27.175 27.35
2.5 3 3.5 4 4.5 5
34.05 34.1 34.15 34.2 34.25

Figure 12